Editors' Suggestion

Symmetry analysis of cross-circular and parallel-circular Raman optical activity

Hikaru Watanabe,[1,*] Rikuto Oiwa,[2,3] Gakuto Kusuno,[4] Takuya Satoh,[4,5] and Ryotaro Arita[1,3]

[1]*Department of Physics, University of Tokyo, Tokyo 113-0033, Japan*

[2]*Department of Physics, Hokkaido University, Sapporo, Hokkaido 113-8656, Japan*

[3]*Center for Emergent Matter Science, RIKEN, Wako, Saitama 351-0198, Japan*

[4]*Department of Physics, Institute of Science Tokyo, Tokyo 152-8551, Japan*

[5]*Quantum Research Center for Chirality, Institute for Molecular Science, Aichi 444-8585, Japan*

(Received 29 June 2025; accepted 14 August 2025; published 2 September 2025)

Raman scattering with regard to circularly polarized incident and scattered lights is closely related to the circular activity of a given system. We investigate the symmetry of its activity, called the cross-circular and parallel-circular Raman optical activity. The analysis is systematically performed with the magnetic point groups, and it indicates that the response allows for a useful diagnosis of the symmetry of materials such as chirality and (magneto)axiality. It is also shown that the Stokes and anti-Stokes processes are related to each other by the conserved antiunitary symmetry, which can be either the time-reversal operation or the combination of time-reversal and mirror reflection.

DOI: 10.1103/45jq-j23c

I. INTRODUCTION

Raman scattering—light scattering with a slight frequency shift—is one of the most powerful probes of materials. The response serves to characterize elementary excitations such as magnons and excitons, and it has been applied to a broad range of fields [1,2]. For instance, the Raman spectroscopy of magnetic materials points to the spectral weight of the state and the electrical activity of magnetic excitations [3–5]. Recent studies have revealed that spectroscopy provides a deeper insight into spontaneous symmetry breaking when combined with control of the polarization of light. It has been shown that Raman spectroscopy can be used to investigate the order parameter and its coupling to the structural and electronic properties of microscaled samples such as van der Waals materials by using circularly polarized and crossed linearly polarized lights [6–11]. In particular, the cross-circular and parallel-circular Raman spectroscopy of our focus is an established method for corroborating the phase of matter.

Figure 1 depicts the setup of cross-circular and parallel-circular Raman spectroscopy in backward scattering geometry. The activity, namely cross- and parallel-circular Raman optical activities (CCROA, PCROA), is found in ferromagnetic materials [10,12,13], nonmagnetic but mirror-asymmetric systems [14–18], and those with chiral structures [19–21].[1] In light of the microscopic mechanism, these Raman optical activities (ROA), termed dual-circular ROA [23], are related to antisymmetric Raman scattering [24,25] and vibronic Raman optical activity [26–28] stemming from the resonant particle-hole excitations and symmetry breaking.

Only recently, the Raman spectroscopic study in Ref. [29] clarified that conserved time-reversal symmetry is tied to the relationship between Stokes and anti-Stokes processes, which refer, respectively, to the emission and absorption of elementary excitation during light scattering. Experimental evidence implies that dual-circular Raman spectroscopy allows us to identify the symmetry, including that of the time-reversal operation with which we are concerned. However, a systematic symmetry analysis has not been presented.

In this work, we present a symmetry analysis of dual-circular ROA. The classification based on magnetic point groups allows us to identify materials with these ROA, and it points to the importance of antiunitary symmetry. Although prior studies tabulated the symmetry-adapted Raman response [30,31], our analysis shows that magnetic symmetry can be used to identify the relationship between Stokes and anti-Stokes processes (creation and annihilation of elementary excitations during light scattering). The classification is based on the magnetic Laue, achiral, and chiral classes, providing a diagnosis of quantum materials manifesting exotic symmetry breaking.

The outline of the paper is as follows. Section II introduces the setup we are interested in, and it explains the symmetry constraints on the Raman-scattering intensity. In Secs. III and IV, we classify the CCROA characteristics of centrosymmetric and noncentrosymmetric materials, respectively. The classification can work in the case of PCROA as well. We discuss the CCROA and PCROA of cubic systems in Sec. V, while the preceding sections are dedicated to an analysis of noncubic crystals. We summarize our work and comment on its implications in Sec. VI.

II. SETUP

We present the symmetry analysis of the (spontaneous) Raman scattering process. Let the light be parametrized by

*Contact author: hikaru-watanabe@g.ecc.u-tokyo.ac.jp

[1]The parallel-circular and cross-circular optical activities are also referred to as activities regarding in-phase dual circular polarization and out-of-phase dual circular polarization, respectively [22].

$(\boldsymbol{e}_X, \omega_X, \boldsymbol{q}_X)$, where $\boldsymbol{e}$ is the polarization vector, ω is the frequency, and $\boldsymbol{q}$ is the wave vector ($X = \mathrm{i}$ for the incident light and $X = \mathrm{f}$ for the scattered light). In the following, we consider the Raman scattering process concerning an elementary excitation $\phi(\delta\omega, \boldsymbol{k})$ such as a phonon and a magnon. The scattering intensities are expressed by [1]

$$U \propto \left|\boldsymbol{e}_{\mathrm{f}}^{\dagger}\hat{\chi}\boldsymbol{e}_{\mathrm{i}}\right|^2 n_{\phi}^{\mathrm{S}}(\delta\omega, \boldsymbol{k}; O) \tag{1}$$

for the Stokes process ($\omega_{\mathrm{i}} > \omega_{\mathrm{s}}$) and

$$U \propto \left|\boldsymbol{e}_{\mathrm{f}}^{\dagger}\hat{\xi}\boldsymbol{e}_{\mathrm{i}}\right|^2 n_{\phi}^{\mathrm{AS}}(\delta\omega, \boldsymbol{k}; O) \tag{2}$$

for the anti-Stokes process ($\omega_{\mathrm{i}} < \omega_{\mathrm{s}}$). Note that the energy and momentum conservations hold as $\omega_{\mathrm{i}} = \omega_{\mathrm{f}} \pm \delta\omega$ and $\boldsymbol{q}_{\mathrm{i}} = \boldsymbol{q}_{\mathrm{f}} \pm \boldsymbol{k}$ for the Stokes and anti-Stokes processes. $\hat{\chi}$ and $\hat{\xi}$ are the nonlinear susceptibilities that describe the emission and absorption of ϕ during the light scattering process. n_{ϕ}^{S} and n_{ϕ}^{AS} are the power spectra denoting the thermal population of ϕ. The power spectra depend on O, that is, the property of the target material such as crystal structure and spontaneous order. For simplicity, we neglected other prefactors such as refractive indices by considering small detuning $|\delta\omega| \ll |\omega|$. The symmetry of light-matter interaction is built into the nonlinear susceptibilities. Let us consider $\hat{\chi}$ written with its parameter dependence as

$$\chi_{ab}(\omega_{\mathrm{i}}, \boldsymbol{q}_{\mathrm{i}}; \delta\omega, \boldsymbol{k}; \mathcal{S}) = \left\langle e_a^{\mathrm{f}}, \omega_{\mathrm{f}}, \boldsymbol{q}_{\mathrm{f}}; \phi(\delta\omega, \boldsymbol{k}) \,\middle|\, \mathcal{S} \,\middle|\, e_b^{\mathrm{i}}, \omega_{\mathrm{i}}, \boldsymbol{q}_{\mathrm{i}} \right\rangle. \tag{3}$$

The operator $\mathcal{S} = \mathcal{S}(O)$ denotes the scattering process with its implicit dependence on O.

The polarization state of light is defined with the circular coordinates, i.e., $\boldsymbol{e}_{\mathrm{R}} = (1, i, 0)/\sqrt{2}$ and $\boldsymbol{e}_{\mathrm{L}} = (1, -i, 0)/\sqrt{2}$ for the right-handed and left-handed circularly polarized lights. As a result, the components of $\hat{\chi}$ are written down by such as χ_{RL}. The circular polarization is given according to the observatory frame, not by the helicity of light (see Fig. 1). Then, we define the cross-circular and parallel-circular Raman optical activities by the difference of the intensities between $(\boldsymbol{e}_{\mathrm{i}}, \boldsymbol{e}_{\mathrm{f}}) = (\boldsymbol{e}_{\mathrm{R}}, \boldsymbol{e}_{\mathrm{L}})$ and $(\boldsymbol{e}_{\mathrm{i}}, \boldsymbol{e}_{\mathrm{f}}) = (\boldsymbol{e}_{\mathrm{L}}, \boldsymbol{e}_{\mathrm{R}})$ in the cross-circular arrangement [Fig. 1(a)], and that between $(\boldsymbol{e}_{\mathrm{i}}, \boldsymbol{e}_{\mathrm{f}}) = (\boldsymbol{e}_{\mathrm{R}}, \boldsymbol{e}_{\mathrm{R}})$ and $(\boldsymbol{e}_{\mathrm{i}}, \boldsymbol{e}_{\mathrm{f}}) = (\boldsymbol{e}_{\mathrm{L}}, \boldsymbol{e}_{\mathrm{L}})$ in the parallel-circular arrangement [Fig. 1(b)], respectively.

Specifically, following reported experimental works, we consider the backward reflection geometry, where the light perpendicularly incident on the sample surface is antiparallel to the scattered light ($\boldsymbol{q}_{\mathrm{i}} = q_i\hat{z}, \boldsymbol{q}_{\mathrm{f}} = -q_i\hat{z}$). We aim to identify the relation between dual-circular Raman optical activity and the bulk symmetry of a given material. To eliminate spurious effects such as the birefringence effect and misalignment of the incident direction from the optical axes [32–34], we assume that the light is propagating along the principal axis $\hat{z}$ of the system. We also assume that the system is noncubic, while we present the symmetry considerations for the cubic point groups later (Sec. V).[2]

Let us consider the symmetry constraint on the nonlinear susceptibilities χ_{ab} and ξ_{ab}. Since we are interested in the backscattering geometry, it suffices to consider an operation g that does not rotate the incident plane, i.e., the symmetry constraints originate from the space-inversion ($g = I$), the n-fold rotation normal to the incident plane ($g = n$), the twofold rotation parallel to the incident plane ($g = 2_{\perp}$), time-reversal operation ($g = \theta$), and combinations of the aforementioned operations such as $g = \theta I$.

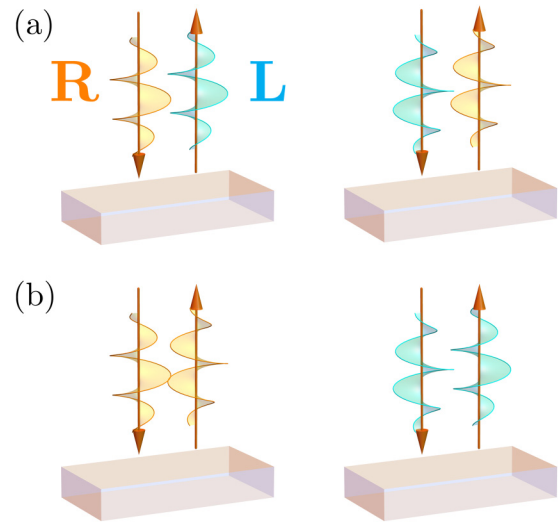

FIG. 1. Experimental setup for measuring (a) the cross-circular Raman optical activity and (b) the parallel-circular Raman optical activity. The orange-colored arrows denote incident and reflected lights. The circular polarization is defined by the rotation direction of the photoelectric field, colored in orange and cyan for right-handed and left-handed polarizations, in a plane fixed in the observatory frame. The optical activities are defined by the difference in the measured quantities between the left and right panels in each of (a) and (b).

First, we consider the space-inversion operation. The susceptibility χ_{ab} for the Stokes process is transformed as

$$\begin{aligned}
&\chi_{ab}(\omega_{\mathrm{i}}, \boldsymbol{q}_{\mathrm{i}}; \delta\omega, \boldsymbol{k}; \mathcal{S}) \\
&= \left\langle e_a^{\mathrm{f}}, \omega_{\mathrm{f}}, \boldsymbol{q}_{\mathrm{f}}; \phi(\delta\omega, \boldsymbol{k}) \,\middle|\, \mathcal{S} \,\middle|\, e_b^{\mathrm{i}}, \omega_{\mathrm{i}}, \boldsymbol{q}_{\mathrm{i}} \right\rangle && (4)\\
&= \left\langle \hat{I}e_a^{\mathrm{f}}, \omega_{\mathrm{f}}, -\boldsymbol{q}_{\mathrm{f}}; \hat{I}\phi(\delta\omega, \boldsymbol{k}) \,\middle|\, \hat{I}\mathcal{S}\hat{I}^{-1} \,\middle|\, \hat{I}e_b^{\mathrm{i}}, \omega_{\mathrm{i}}, -\boldsymbol{q}_{\mathrm{i}} \right\rangle && (5)\\
&= \rho_I \left\langle e_a^{\mathrm{f}}, \omega_{\mathrm{f}}, -\boldsymbol{q}_{\mathrm{f}}; \phi(\delta\omega, -\boldsymbol{k}) \,\middle|\, \hat{I}\mathcal{S}\hat{I}^{-1} \,\middle|\, e_b^{\mathrm{i}}, \omega_{\mathrm{i}}, -\boldsymbol{q}_{\mathrm{i}} \right\rangle && (6)\\
&= \rho_I \chi_{ab}(\omega_{\mathrm{i}}, -\boldsymbol{q}_{\mathrm{i}}; \delta\omega, -\boldsymbol{k}; \hat{I}\mathcal{S}\hat{I}^{-1}), && (7)
\end{aligned}$$

where ρ_I denotes the I parity of ϕ. If $\hat{I}\mathcal{S}\hat{I}^{-1} = \mathcal{S}(\hat{I}O\hat{I}^{-1}) = \mathcal{S}(O)$ holds due to the I symmetry of the system, the scattering event is nonreciprocal, as is evident from the relation

$$\left|\boldsymbol{e}_{\mathrm{f}}^{\dagger}\hat{\chi}(\omega_{\mathrm{i}}, \boldsymbol{q}_{\mathrm{i}}; \delta\omega, \boldsymbol{k}; \mathcal{S})\boldsymbol{e}_{\mathrm{i}}\right|^2 = \left|\boldsymbol{e}_{\mathrm{f}}^{\dagger}\hat{\chi}(\omega_{\mathrm{i}}, -\boldsymbol{q}_{\mathrm{i}}; \delta\omega, -\boldsymbol{k}; \mathcal{S})\boldsymbol{e}_{\mathrm{i}}\right|^2, \tag{8}$$

where the right-hand side denotes the scattering event whose experimental arrangement is the space-inversion (I) image of the original configuration. The total scattering intensity [Eq. (1)] is also nonreciprocal because the I symmetry of O leads to

$$n_{\phi}^{\mathrm{S}}(\delta\omega, \boldsymbol{k}; O) = n_{\phi}^{\mathrm{S}}(\delta\omega, -\boldsymbol{k}; \hat{I}O\hat{I}^{-1}) = n_{\phi}^{\mathrm{S}}(\delta\omega, -\boldsymbol{k}; O). \tag{9}$$

[2]In the case of orthorhombic crystals, there is an ambiguity in choosing the axis from $\hat{x}, \hat{y}, \hat{z}$. We take the $\hat{z}$ axis in this work, but this specific choice does not affect the conclusion.

The purely nonreciprocal property does not hold in I -broken systems. One can decompose the scattering intensity into the nonreciprocal and reciprocal parts as

$$\begin{aligned}&\left|\boldsymbol{e}_{\mathrm{f}}^{\dagger}\hat{\chi}(\omega_{\mathrm{i}},\boldsymbol{q}_{\mathrm{i}};\delta\omega,\boldsymbol{k};\mathcal{S})\boldsymbol{e}_{\mathrm{i}}\right|^2 n_{\phi}^{\mathrm{S}}(\delta\omega,\boldsymbol{k};O)\\&=\tfrac{1}{2}\left\{\left|\boldsymbol{e}_{\mathrm{f}}^{\dagger}\hat{\chi}(\omega_{\mathrm{i}},\boldsymbol{q}_{\mathrm{i}};\delta\omega,\boldsymbol{k};\mathcal{S})\boldsymbol{e}_{\mathrm{i}}\right|^2 n_{\phi}^{\mathrm{S}}(\delta\omega,\boldsymbol{k};O)\right.\\&\quad\left.+\left|\boldsymbol{e}_{\mathrm{f}}^{\dagger}\hat{\chi}(\omega_{\mathrm{i}},-\boldsymbol{q}_{\mathrm{i}};\delta\omega,-\boldsymbol{k};\mathcal{S})\boldsymbol{e}_{\mathrm{i}}\right|^2 n_{\phi}^{\mathrm{S}}(\delta\omega,-\boldsymbol{k};O)\right\}\\&\quad+\tfrac{1}{2}\left\{\left|\boldsymbol{e}_{\mathrm{f}}^{\dagger}\hat{\chi}(\omega_{\mathrm{i}},\boldsymbol{q}_{\mathrm{i}};\delta\omega,\boldsymbol{k};\mathcal{S})\boldsymbol{e}_{\mathrm{i}}\right|^2 n_{\phi}^{\mathrm{S}}(\delta\omega,\boldsymbol{k};O)\right.\\&\quad\left.-\left|\boldsymbol{e}_{\mathrm{f}}^{\dagger}\hat{\chi}(\omega_{\mathrm{i}},-\boldsymbol{q}_{\mathrm{i}};\delta\omega,-\boldsymbol{k};\mathcal{S})\boldsymbol{e}_{\mathrm{i}}\right|^2 n_{\phi}^{\mathrm{S}}(\delta\omega,-\boldsymbol{k};O)\right\}.\end{aligned}\tag{10}$$

The first line is nonreciprocal, and the second line is the reciprocal contribution arising from the I symmetry breaking. By using the I -parity characterization, we define the reciprocal and nonreciprocal dual-circular ROA. For instance, when CCROA of the Stokes process ($\omega_{\mathrm{i}}>\omega_{\mathrm{s}}$) is given by

$$\begin{aligned}&\mathrm{CC}(\omega_{\mathrm{i}},\boldsymbol{q}_{\mathrm{i}};\delta\omega,\boldsymbol{k};O)\\&\equiv\left\{\left|\chi_{\mathrm{LR}}(\omega_{\mathrm{i}},\boldsymbol{q}_{\mathrm{i}};\delta\omega,\boldsymbol{k};\mathcal{S})\right|^2-\left|\chi_{\mathrm{RL}}(\omega_{\mathrm{i}},\boldsymbol{q}_{\mathrm{i}};\delta\omega,\boldsymbol{k};\mathcal{S})\right|^2\right\}\\&\quad\times n_{\phi}^{\mathrm{S}}(\delta\omega,\boldsymbol{k};O),\end{aligned}\tag{11}$$

the nonreciprocal and even-parity contribution is given by

$$\begin{aligned}\mathrm{CC}_{+}(\omega_{\mathrm{i}},\delta\omega,O)\equiv\tfrac{1}{2}\big\{&\mathrm{CC}(\omega_{\mathrm{i}},\boldsymbol{q}_{\mathrm{i}};\delta\omega,\boldsymbol{k};O)\\&+\mathrm{CC}(\omega_{\mathrm{i}},-\boldsymbol{q}_{\mathrm{i}};\delta\omega,-\boldsymbol{k};O)\big\},\end{aligned}\tag{12}$$

while the reciprocal and odd-parity part is

$$\begin{aligned}\mathrm{CC}_{-}(\omega_{\mathrm{i}},\delta\omega,O)\equiv\tfrac{1}{2}\big\{&\mathrm{CC}(\omega_{\mathrm{i}},\boldsymbol{q}_{\mathrm{i}};\delta\omega,\boldsymbol{k};O)\\&-\mathrm{CC}(\omega_{\mathrm{i}},-\boldsymbol{q}_{\mathrm{i}};\delta\omega,-\boldsymbol{k};O)\big\}.\end{aligned}\tag{13}$$

PCROA of the Stokes process is defined by

$$\begin{aligned}\mathrm{PC}(\omega_{\mathrm{i}},\boldsymbol{q}_{\mathrm{i}};\delta\omega,\boldsymbol{k};O)\equiv\big\{&\left|\chi_{\mathrm{RR}}(\omega_{\mathrm{i}},q_i\hat{z};\delta\omega,\boldsymbol{k};\mathcal{S})\right|^2\\&-\left|\chi_{\mathrm{LL}}(\omega_{\mathrm{i}},q_i\hat{z};\delta\omega,\boldsymbol{k};\mathcal{S})\right|^2\big\}\\&\times n_{\phi}^{\mathrm{S}}(\delta\omega,\boldsymbol{k};O),\end{aligned}\tag{14}$$

and its even-parity (PC_{+}) and odd-parity (PC_{-}) terms are obtained in a similar manner to the case of CCROA. Note that the odd-parity dual-circular ROA (CC_{-} and PC_{-}) vanishes if $\hat{I}O\hat{I}^{-1}=O$.

The symmetry analysis of $\hat{\chi}$ is similarly performed in the case of another unitary operation. The important consequence is drawn from the mirror operation $m_{\perp}$, that is, the mirror reflection with respect to the incident plane of light. The operation interchanges the circular polarization of light as $\hat{m}_{\perp}\boldsymbol{e}_{\mathrm{R}}=\boldsymbol{e}_{\mathrm{L}},\hat{m}_{\perp}\boldsymbol{e}_{\mathrm{L}}=\boldsymbol{e}_{\mathrm{R}}$. Thus, if the system is $m_{\perp}$-symmetric, dual-circular ROA is forbidden, e.g., CCROA vanishes as

$$\mathrm{CC}_{X}(\omega_{\mathrm{i}},\delta\omega,O)=-\mathrm{CC}_{X}(\omega_{\mathrm{i}},\delta\omega,O)=0\tag{15}$$

for $X=\pm$. As a result, the systems in which we are interested are those that lack $m_{\perp}$ symmetry. The $m_{\perp}$ breaking occurs with or without the simultaneous I symmetry breaking, which will be discussed in Secs. III and IV, respectively.

Next, we consider the time-reversal (θ) operation. The nonlinear susceptibility χ_{ab} undergoes the transformation as

$$\begin{aligned}&\chi_{ab}(\omega_{\mathrm{i}},\boldsymbol{q}_{\mathrm{i}};\delta\omega,\boldsymbol{k};\mathcal{S})\\&=\left\langle\hat{\theta}e_b^{\mathrm{i}},\omega_{\mathrm{i}},-\boldsymbol{q}_{\mathrm{i}}\,\middle|\,\hat{\theta}\mathcal{S}^{\dagger}\hat{\theta}^{-1}\,\middle|\,\hat{\theta}e_a^{\mathrm{f}},\omega_{\mathrm{f}},-\boldsymbol{q}_{\mathrm{f}};\hat{\theta}\phi(\delta\omega,\boldsymbol{k})\right\rangle\end{aligned}\tag{16}$$

$$=\left\langle e_{\overline{b}}^{\mathrm{i}},\omega_{\mathrm{i}},-\boldsymbol{q}_{\mathrm{i}}\,\middle|\,\overline{\mathcal{S}}\,\middle|\,e_{\overline{a}}^{\mathrm{f}},\omega_{\mathrm{f}},-\boldsymbol{q}_{\mathrm{f}};\overline{\phi}(\delta\omega,-\boldsymbol{k})\right\rangle\tag{17}$$

$$=\xi_{\overline{b}\overline{a}}(\omega_{\mathrm{f}},\boldsymbol{q}_{\mathrm{f}};\delta\omega,\boldsymbol{k};\overline{\mathcal{S}}),\tag{18}$$

where $e_{\overline{b}}\equiv\theta e_b$, $\overline{\mathcal{S}}\equiv\hat{\theta}\mathcal{S}^{\dagger}\hat{\theta}^{-1}$, and $\overline{\phi}=\theta\phi$. The operator $\overline{\mathcal{S}}$, that is, the θ -partner of $\mathcal{S}$, does not violate the causality but shows the opposite polarity in its time-reversal-odd properties such as magnetization [35]. Following Ref. [36], it is shown that the power spectra of ϕ and $\overline{\phi}$ are related as

$$f_{\mathrm{B}}(\delta\omega)n_{\phi}^{\mathrm{S}}(\delta\omega,\boldsymbol{k};O)=\{1+f_{\mathrm{B}}(\delta\omega)\}n_{\overline{\phi}}^{\mathrm{AS}}(\delta\omega,-\boldsymbol{k};\overline{O}),\tag{19}$$

with the Bose-Einstein distribution function $f_{\mathrm{B}}(\delta\omega)$ and $\overline{O}=\hat{\theta}O\hat{\theta}^{-1}$. As a result, the θ operation relates the Stokes and anti-Stokes Raman scattering intensities whose frequency of incident light is ω_{i} and $\omega_{\mathrm{f}}=\omega_{\mathrm{i}}-\delta\omega$, as clarified in Refs. [2,36]. In terms of CCROA, considering $e_{\mathrm{R}}=\hat{\theta}e_{\mathrm{L}}$ and $e_{\mathrm{L}}=\hat{\theta}e_{\mathrm{R}}$, we obtain the relation

$$\begin{aligned}&\mathrm{CC}(\omega_{\mathrm{i}},\boldsymbol{q}_{\mathrm{i}};\delta\omega,\boldsymbol{k};O)\\&=\frac{1+f_{\mathrm{B}}(\delta\omega)}{f_{\mathrm{B}}(\delta\omega)}\mathrm{CC}(\omega_{\mathrm{f}},-\boldsymbol{q}_{\mathrm{f}};-\delta\omega,-\boldsymbol{k};\overline{O}),\end{aligned}\tag{20}$$

where CCROA with $-\delta\omega<0$ (right-hand side) is defined by the anti-Stokes scattering intensities as

$$\begin{aligned}\mathrm{CC}(\omega_{\mathrm{f}},-\boldsymbol{q}_{\mathrm{f}};-\delta\omega,-\boldsymbol{k};\overline{O})=\big\{&\left|\xi_{\mathrm{LR}}(\omega_{\mathrm{f}},-\boldsymbol{q}_{\mathrm{f}};\delta\omega,-\boldsymbol{k};\overline{\mathcal{S}})\right|^2\\&-\left|\xi_{\mathrm{RL}}(\omega_{\mathrm{f}},-\boldsymbol{q}_{\mathrm{f}};\delta\omega,-\boldsymbol{k};\overline{\mathcal{S}})\right|^2\big\}\\&\times n_{\overline{\phi}}^{\mathrm{AS}}(\delta\omega,-\boldsymbol{k};\overline{O}).\end{aligned}\tag{21}$$

Since the detuning frequency $\delta\omega=|\omega_{\mathrm{i}}-\omega_{\mathrm{f}}|$ is much smaller than the frequency of light ω_{i}, we may approximate Eq. (20) as

$$\mathrm{CC}(\omega_{\mathrm{i}},\boldsymbol{q}_{\mathrm{i}};\delta\omega,\boldsymbol{k};O)\approx\frac{1+f_{\mathrm{B}}(\delta\omega)}{f_{\mathrm{B}}(\delta\omega)}\mathrm{CC}(\omega_{\mathrm{i}},\boldsymbol{q}_{\mathrm{i}};-\delta\omega,-\boldsymbol{k};\overline{O}),\tag{22}$$

which indicates the symmetry of CCROA in the Stokes and anti-Stokes processes whose systems are parametrized by O and $\overline{O}$, respectively. We also used $\boldsymbol{q}_{\mathrm{f}}=-\boldsymbol{q}_{\mathrm{i}}$.

If the system is θ -symmetric, $\overline{O}=O$ holds, resulting in the same signs between the Stokes and anti-Stokes CCROA as

$$\mathrm{CC}(\omega_{\mathrm{i}},\boldsymbol{q}_{\mathrm{i}};\delta\omega,\boldsymbol{k};O)\approx\frac{1+f_{\mathrm{B}}(\delta\omega)}{f_{\mathrm{B}}(\delta\omega)}\mathrm{CC}(\omega_{\mathrm{i}},\boldsymbol{q}_{\mathrm{i}};-\delta\omega,-\boldsymbol{k};O).\tag{23}$$

Furthermore, the combined operation of θ and $m_{\perp}$ leads to the relation complementary to Eq. (20). In the case of CCROA, the following relation is obtained:

$$\begin{aligned}&\mathrm{CC}(\omega_{\mathrm{i}},\boldsymbol{q}_{\mathrm{i}};\delta\omega,\boldsymbol{k};O)\\&=-\frac{1+f_{\mathrm{B}}(\delta\omega)}{f_{\mathrm{B}}(\delta\omega)}\mathrm{CC}(\omega_{\mathrm{f}},-\boldsymbol{q}_{\mathrm{f}};-\delta\omega,-\boldsymbol{k};\overline{O}')\end{aligned}\tag{24}$$

$$\approx-\frac{1+f_{\mathrm{B}}(\delta\omega)}{f_{\mathrm{B}}(\delta\omega)}\mathrm{CC}(\omega_{\mathrm{i}},\boldsymbol{q}_{\mathrm{i}};-\delta\omega,-\boldsymbol{k};\overline{O}'),\tag{25}$$

where $\overline{O}'=\hat{\theta}\hat{m}_{\perp}O^{\dagger}(\hat{\theta}\hat{m}_{\perp})^{-1}$. As a result, a $\theta m_{\perp}$-symmetric system may show Stokes and anti-Stokes CCROA with opposite signs, which is in stark contrast to the θ -symmetric

systems. Note that the $\theta m_\perp$-symmetric part of CCROA is forbidden if the system also respects the θ symmetry because of the conserved $m_\perp$ symmetry [see Eq. (15)]. Thus, the obtained contribution is unique to θ -broken systems.

To summarize, CCROA consists of four contributions as follows. First, it is divided into the even- and odd-parity parts as

$$\mathrm{CC}_+(\omega_\mathrm{i}, \delta\omega, O) + \mathrm{CC}_-(\omega_\mathrm{i}, \delta\omega, O). \tag{26}$$

Each part is further classified into the θ-even and θ-odd contributions, which manifest the same (symmetric) and opposite (antisymmetric) signs between the Stokes and anti-Stokes signals, respectively. In light of the θ parity, CC_X is decomposed as

$$\mathrm{CC}_X(\omega_\mathrm{i}, \delta\omega, O) = \mathrm{CC}_X^\mathrm{s}(\omega_\mathrm{i}, \delta\omega, O) + \mathrm{CC}_X^\mathrm{a}(\omega_\mathrm{i}, \delta\omega, O), \tag{27}$$

where CC_+^s is θ-even ($\theta m_\perp$-odd) and CC_+^a is θ-odd ($\theta m_\perp$-even).

Following the parallel discussions, PCROA is classified by the parity with respect to the I and θ operations. PCROA, however, differs from CCROA in terms of the Stokes and anti-Stokes symmetries ensured by the θ or $\theta m_\perp$ symmetry; in θ -symmetric systems,

$$\begin{aligned}&\mathrm{PC}(\omega_\mathrm{i}, \boldsymbol{q}_\mathrm{i}; \delta\omega, \boldsymbol{k}; O)\\ &\quad\approx -\frac{1+f_\mathrm{B}(\delta\omega)}{f_\mathrm{B}(\delta\omega)}\mathrm{PC}(\omega_\mathrm{i}, \boldsymbol{q}_\mathrm{i}; -\delta\omega, -\boldsymbol{k}; O),\end{aligned} \tag{28}$$

exhibiting the opposite signs between the emission and absorption processes. On the other hand, if the $\theta m_\perp$ symmetry is intact, the following relation holds:

$$\mathrm{PC}(\omega_\mathrm{i}, \boldsymbol{q}_\mathrm{i}; \delta\omega, \boldsymbol{k}; O) \approx \frac{1+f_\mathrm{B}(\delta\omega)}{f_\mathrm{B}(\delta\omega)}\mathrm{PC}(\omega_\mathrm{i}, \boldsymbol{q}_\mathrm{i}; -\delta\omega, -\boldsymbol{k}; O). \tag{29}$$

Then, the θ-even term is labeled by the antisymmetric PCROA (PC_X^a), while the θ-odd term is labeled by the symmetric part (PC_X^s).

As a result, the symmetry between the Stokes and anti-Stokes signals is contrasting between the θ -symmetric system and θ-violating but $\theta m_\perp$-conserving system. It implies that careful observation of Stokes and anti-Stokes signals enables us to identify the antiunitary symmetry in materials. Note that, when both the θ and $\theta m_\perp$ symmetries are broken, both the symmetric and antisymmetric components are allowed. Similar arguments are found in Ref. [37] investigating CCROA and PCROA of the chiral molecules as well as in discussions concerning another type of ROA for the odd-parity and θ-even [38,39] and the even-parity and θ-odd cases [40]. On the other hand, our symmetry analysis further generalizes their discussions to cover more diverse cases, e.g., the even-parity and θ-even or odd-parity and θ-odd dual-circular ROA, which are not realized in molecular gas and solution. In the following sections, however, we generalize their results from the viewpoint of symmetry and classify all the magnetic point groups in terms of the I and θ parts of CCROA and PCROA.

III. EVEN-PARITY CROSS-CIRCULAR RAMAN OPTICAL ACTIVITY

We consider the even-parity CCROA (CC_+) to delve into the symmetry of the Raman scattering process. The I-operation constraint [Eq. (7)] leads to the relation

$$\mathrm{CC}_+(\omega, \delta\omega, O) = \mathrm{CC}_+(\omega, \delta\omega, IOI^{-1}). \tag{30}$$

Thus, the even-parity part is identical between the original system (O) and its inversion motif (IOI^{-1}), after which the point group of the target material $\boldsymbol{G}$ shows the same CC_+ symmetry as that of the point group enhanced by the space-inversion operation $\boldsymbol{G} \cup I\boldsymbol{G}$.

The classification of CC_+ is therefore given by the Laue class, a series of point groups that are merged into the same group after the inversion-operation enhancement. For instance, the trigonal point groups are classified into the Laue classes $\bar{3}$ and $\bar{3}m$. They are explicitly given as

$$\bar{3} = \{3, \bar{3}\},\ \bar{3}m = \{32, 3m, \bar{3}m\}.$$

The former class does not show the $m_\perp$ symmetry, while the latter does. As a result, the even-parity CCROA is allowed in the $\bar{3}$-class materials, while it is forbidden in the $\bar{3}m$-class materials.

Furthermore, Eqs. (22) and (25) imply that the antiunitary operation relates the CC_+ of the Stokes process with that of the anti-Stokes process. Thus, it is convenient to classify the response in terms of the magnetic point groups. 122 magnetic point groups are classified into the magnetic-group analog of the Laue class, that is, the magnetic Laue class. Similarly to the magnetic point groups, the magnetic Laue class is defined by the series of magnetic point groups merged by the space-inversion operation. The magnetic Laue classes are classified into three types as in the case of magnetic point groups: colorless, gray, and black-white Laue classes. The colorless class does not have any antiunitary element like θ.

The gray and black-white Laue classes for trigonal systems are obtained as

$$\begin{aligned}&\bar{3}1' = \{31', \bar{3}1', \bar{3}'\},\\ &\bar{3}m1' = \{321', 3m1', \bar{3}m1', \bar{3}'m, \bar{3}m'\},\\ &\bar{3}m' = \{32', 3m', \bar{3}m'\}.\end{aligned}$$

Note that the gray Laue class can cover black-white point groups. For instance, the magnetic point group $\bar{3}'$ is included in the gray Laue class $\bar{3}1'$. We obtained the five magnetic Laue classes for the trigonal system in total. Due to the $m_\perp$ symmetry, the classes $\bar{3}m$ and $\bar{3}m1'$ do not have activity concerning CC_+, while the rest of the classes ($\bar{3}$, $\bar{3}1'$, $\bar{3}m'$) do.

For the gray Laue class $\bar{3}1'$, CCROA is attributed to CC_+^s because of the θ symmetry. Materials belonging to this class are found in a series of so-called ferroaxial (ferrorotational) materials where the ferroaxial vector $\boldsymbol{A}$, a θ-even axial vector implying the $m_\perp$-symmetry violation, can be present due to their crystal structures or structural phase transition [41–47]. Candidate materials undergoing the ferroaxial phase transition include $RbFe(MoO_4)_2$ [44,48,49], $K_2Zr(PO_4)_2$ [44,45], $NiTiO_3$ [50], $MnTiO_3$ [51,52], $Ca_5Ir_3O_{12}$ [53–55], $Na_2BaM(PO_4)_2$ [56,57], van der Waals materials in the charge-density-wave phase [14–17,58], and so on. Being

consistent with the symmetry analysis, the same sign of the CCROA signals between the Stokes and anti-Stokes signals has been observed [29].

On the other hand, the black-white Laue class $\bar{3}m'$ allows for the θ-odd and antisymmetric part of the even-parity CCROA denoted by $\mathrm{CC}_+^{\mathrm{a}}$. The response is not admixed with the θ-even counterpart $\mathrm{CC}_+^{\mathrm{s}}$ because of the $\theta m_\perp$ symmetry. The black-white Laue class shows the magnetoaxial symmetry whose unitary symmetry is the same as that of the ferroaxial system, but θ symmetry is not kept without combining with the $m_\perp$ or $2_\perp$ operation. The magnetoaxial symmetry is found in ferromagnetic systems. Experimental observations have been made in ferromagnets [10,12,13] and systems under the external magnetic field [59,60]. Note that the activity can be present in not only the ferromagnets but also the antiferromagnets manifesting the magnetoaxial symmetry, like Mn_3Sn [61,62]. Both the θ-even and θ-odd CC_+ activities coexist in the colorless Laue class $\bar{3}$.

The classification based on the (noncubic) magnetic Laue class is completed in Table I. Some of the black-white Laue classes allow for both $\mathrm{CC}_+^{\mathrm{s}}$ and $\mathrm{CC}_+^{\mathrm{a}}$ because of the ferroaxial motif of their crystal structure.

IV. ODD-PARITY CROSS-CIRCULAR RAMAN OPTICAL ACTIVITY

The odd-parity CCROA (CC_-) undergoes the I -operation transformation as

$$\mathrm{CC}_-(\omega, \delta\omega, O) = -\mathrm{CC}_-(\omega, \delta\omega, IOI^{-1}). \tag{31}$$

Combining the constraint from the out-of-plane mirror reflection $m_\perp$, the odd-parity CCROA does not differ in systems with O and with its rotation image $2_\perp O 2_\perp^{-1}$ ($2_\perp = I \times \mathrm{m}_\perp$);

$$\mathrm{CC}_-(\omega, \delta\omega, O) = \mathrm{CC}_-(\omega, \delta\omega, 2_\perp O 2_\perp^{-1}). \tag{32}$$

In conjunction with discussions on the even-parity CCROA, let us make use of the class of the point groups merged by the out-of-plane twofold rotation.

For instance, the magnetic point groups for trigonal systems are classified into the five classes

$$32 = \{3, 32\}, \tag{33}$$

$$\bar{3}m = \{3m, \bar{3}, \bar{3}m\}, \tag{34}$$

$$321' = \{31', 321', 32'\}, \tag{35}$$

$$\bar{3}m1' = \{3m1', \bar{3}1', \bar{3}m1', \bar{3}m', \bar{3}'m\}, \tag{36}$$

$$\bar{3}'m' = \{\bar{3}', 3m', \bar{3}'m'\}. \tag{37}$$

The obtained classes are as follows. The chiral class $321'$ has θ symmetry but no improper rotation and is characterized by the θ-even pseudoscalar [63]. The black-white class $\bar{3}'m'$ also has no improper rotation in its unitary operations but conserves the θI symmetry, which forbids the θ-even pseudoscalar. On the other hand, the θ-odd and θI -even pseudoscalar, namely magnetic chirality, is allowed in $\bar{3}'m'$. The chiral class $321'$ is characterized by $\mathrm{CC}_-^{\mathrm{s}}$, while the $\bar{3}'m'$ in the magnetic chiral class allows for only $\mathrm{CC}_-^{\mathrm{a}}$ because the preserved θI symmetry forbids the θ-even CCROA ($\mathrm{CC}_-^{\mathrm{s}}$). Two types of odd-parity

TABLE I. Classification of the even-parity cross-circular Raman optical activity (CC_+) by magnetic Laue class. Each class is labeled by the θ-even and θ-odd CCROA; e.g., $(\times, \checkmark)$ denotes no θ-even CCROA but allowed θ-odd CCROA. The magnetic Laue class is comprised of magnetic point groups ($M = G$ or $M = G \cup \theta g G$) in which unitary operations g form the group G and antiunitary operations are given by $\theta g G$. CCROA with the superscript "$*$" denotes what may be admixed with the birefringence effect.

Laue class	CCROA	M	G	g
(colorless Laue class)				
$\bar{1}$	$(\checkmark, \checkmark)^*$	1	1	
		$\bar{1}$	$\bar{1}$	
$2/m$	$(\checkmark, \checkmark)^*$	2	2	
		m	m	
		$2/m$	$2/m$	
mmm	$(\times, \times)$	$2mm$	$2mm$	
		222	222	
		mmm	mmm	
$\bar{3}$	$(\checkmark, \checkmark)$	3	3	
		$\bar{3}$	$\bar{3}$	
$\bar{3}m$	$(\times, \times)$	32	32	
		$3m$	$3m$	
		$\bar{3}m$	$\bar{3}m$	
$4/m$	$(\checkmark, \checkmark)$	4	4	
		$\bar{4}$	$\bar{4}$	
		$4/m$	$4/m$	
$6/m$	$(\checkmark, \checkmark)$	6	6	
		$\bar{6}$	$\bar{6}$	
		$6/m$	$6/m$	
$4/mmmm$	$(\times, \times)$	422	422	
		$4mm$	$4mm$	
		$\bar{4}2m$	$\bar{4}2m$	
		$4/mmm$	$4/mmm$	
$6/mmmm$	$(\times, \times)$	622	622	
		$6mm$	$6mm$	
		$\bar{6}2m$	$\bar{6}2m$	
		$6/mmm$	$6/mmm$	
(gray and black-white Laue classes)				
$\bar{1}1'$	$(\checkmark, \times)^*$	$1'$	1	1
		$\bar{1}1'$	$\bar{1}$	1
		$\bar{1}'$	1	$\bar{1}$
$2/m1'$	$(\checkmark, \times)^*$	$21'$	2	1
		$m1'$	m	1
		$2/m1'$	$2/m$	1
		$2/m'$	2	m
		$2'/m$	m	2
$2'/m'$	$(\checkmark, \checkmark)^*$	m'	1	m
		$2'$	1	2
		$2'/m'$	$\bar{1}$	2
$mmm1'$	$(\times, \times)$	$2mm1'$	$2mm$	1
		$2221'$	222	1
		$mmm1'$	mmm	1
		$m'm'm'$	222	$\bar{1}$
		$m'mm$	$2mm$	$\bar{1}$
$m'mm$	$(\times, \checkmark)$	$2'2'2$	2	1
		$m'm'2$	2	m
		$m'm2'$	m	2
		$m'mm$	$2/m$	2
$\bar{3}1'$	$(\checkmark, \times)$	$31'$	3	1
		$\bar{3}1'$	$\bar{3}$	1
		$\bar{3}'$	3	$\bar{1}$

TABLE I. (*Continued.*)

Laue class	CCROA	M	G	g
$\bar{3}m1'$	$(\times,\times)$	$321'$	32	1
		$3m1'$	$3m$	1
		$\bar{3}m1'$	$\bar{3}m$	1
		$\bar{3}'m$	$3m$	$\bar{1}$
		$\bar{3}'m'$	32	$\bar{1}$
$\bar{3}m'$	$(\times,\checkmark)$	$32'$	3	$2_\perp$
		$3m'$	3	$m_\perp$
		$\bar{3}m'$	$\bar{3}$	$m_\perp$
$4/m1'$	$(\checkmark,\times)$	$41'$	4	1
		$\bar{4}1'$	$\bar{4}$	1
		$4/m1'$	$4/m$	1
		$4/m'$	4	$\bar{1}$
		$4'/m'$	$\bar{4}$	$\bar{1}$
$4'/m$	$(\checkmark,\checkmark)$	$4'$	2	4
		$\bar{4}'$	2	$\bar{4}$
		$4'/m$	$2/m$	$\bar{4}$
$6/m1'$	$(\checkmark,\times)$	$61'$	6	1
		$\bar{6}1'$	$\bar{6}$	1
		$6/m1'$	$6/m$	1
		$6/m'$	6	$\bar{1}$
		$6'/m$	$\bar{6}$	$\bar{1}$
$6'/m'$	$(\checkmark,\checkmark)$	$\bar{6}'$	3	m
		$6'$	3	2
		$6'/m'$	$\bar{3}$	2
$4/mmm1'$	$(\times,\times)$	$4221'$	422	1
		$4mm1'$	$4mm$	1
		$\bar{4}2m1'$	$\bar{4}2m$	1
		$4/mmm1'$	$4/mmm$	1
		$4/m'm'm'$	422	$\bar{1}$
		$4/m'mm$	$4mm$	$\bar{1}$
		$4'/m'm'm$	$\bar{4}2m$	$\bar{1}$
$4'/mmm'$	$(\times,\times)$	$4'22'$	222	$2_\perp$
		$4'mm'$	$2mm$	$2_\perp$
		$\bar{4}'2m'$	222	$m_\perp$
		$\bar{4}'2'm$	$2mm$	$m_\perp$
		$4'/mmm'$	mmm	$2_\perp$
$4/mm'm'$	$(\times,\checkmark)$	$4m'm'$	4	$m_\perp$
		$42'2'$	4	$2_\perp$
		$\bar{4}2'm'$	$\bar{4}$	$m_\perp$
		$4/mm'm'$	$4/m$	$2_\perp$
$6/mmm1'$	$(\times,\times)$	$6221'$	622	1
		$6mm1'$	$6mm$	1
		$\bar{6}2m1'$	$\bar{6}2m$	1
		$6/mmm1'$	$6/mmm$	1
		$6'/mmm'$	$\bar{6}m2$	$\bar{1}$
		$6/m'm'm'$	622	$\bar{1}$
		$6/m'mm$	$6mm$	$\bar{1}$
$6/mm'm'$	$(\times,\checkmark)$	$\bar{6}m'2'$	$\bar{6}$	$2_\perp$
		$\bar{6}'m'2$	32	$m_\perp$
		$62'2'$	6	$2_\perp$
		$6m'm'$	6	$m_\perp$
		$6/mm'm'$	$6/m$	$m_\perp$
$6'/m'm'm$	$(\times,\times)$	$\bar{6}'m2'$	$3m$	$2_\perp$
		$6'2'2$	32	$2_\perp$
		$6'm'm$	32	$m_\perp$
		$6'/m'm'm$	$\bar{3}m$	2

CCROA are concurrently allowed in the colorless class 32, which shows the chirality as well as the magnetic chirality and hence can be called the composite-chiral class.

CCROA for the chiral class has been confirmed in systems with chiral motifs such as the chiral solids and molecules [19,21–23,64]. The Stokes and anti-Stokes parts of CCROA observed in [19,21] are consistent with the formula for $\mathrm{CC}_-^{\mathrm{s}}$ [38,39]. On the other hand, they show the opposite signs in materials belonging to the magnetic chiral class, such as the θI -symmetric magnets, Cr_2O_3, even-layered $MnBi_2Te_4$, and so on [65].

In contrast to the noncentrosymmetric classes, the class $\bar{3}m1'$ is achiral and shows θ symmetry and improper rotation symmetries. Finally, the colorless class $\bar{3}m$ similarly shows improper rotation symmetry without any antiunitary symmetry such as θ, implying magnetic achiral symmetry. The achiral and magnetoachiral classes do not show the odd-parity CCROA due to their $m_\perp$ or I symmetry.

We show the classification table of CC_- in Table II for the noncubic magnetic point groups. Supposing that the symmetry of a magnetic point group is enhanced as long as its holohedry is maintained [66], we obtained each class by using the n-fold ($g = n$) and twofold ($g = 2_\perp$) rotations, which are parallel and perpendicular to the principal axis, respectively.

We also show a summary of CCROA and PCROA in Fig. 2. The response is divided into four types in terms of the parity under the I and θ operations. Note that, similarly to the case of CCROA, PCROA is classified based on the magnetic Laue and a series of chiral and achiral classes. Different types of ROA can be admixed with each other in those with significant symmetry violations; e.g., in the case of the θ-even CCROA, a chiral and ferroaxial crystal can host both $\mathrm{CC}_+^{\mathrm{s}}$ and $\mathrm{CC}_-^{\mathrm{s}}$ [18].

V. CCROA AND PCROA OF CUBIC SYSTEMS

We did not perform a symmetry analysis for the cubic systems in the previous sections because the primary direction cannot be chosen without ambiguity. Let us take several incident directions and consider the symmetry of CCROA for cubic systems in the normal reflection geometry. The symmetry of PCROA can be derived from that of CCROA.

To prevent the response from being admixed with the birefringence effect, the incident direction $\boldsymbol{q}_{\mathrm{i}}$ is taken to be the high symmetry rotation axes with the n-fold rotation symmetry ($n \geqslant 3$). The candidates are [001], [111], and their crystallographically equivalent axes of the cubic systems in the conventional setting. We consider the even-parity and odd-parity CCROA for the [001] and [111] incident directions as follows.

In the case of $\boldsymbol{q}_{\mathrm{i}} = [001]$ incidence, CCROA is forbidden in the presence of the $m_\perp$ symmetry whose mirror plane contains the [001] axis. Similarly to the case of noncubic systems, the even-parity CCROA is classified by the magnetic Laue class for cubic point groups. We tabulate these classes as

$$m\bar{3},\ m\bar{3}m,\ m\bar{3}1',\ m\bar{3}m1',\ m\bar{3}m'. \tag{38}$$

Every class contains the $m_\perp$ or $2_\perp = Im_\perp$ symmetry-forbidden CCROA regarding the [001] incidence. It follows

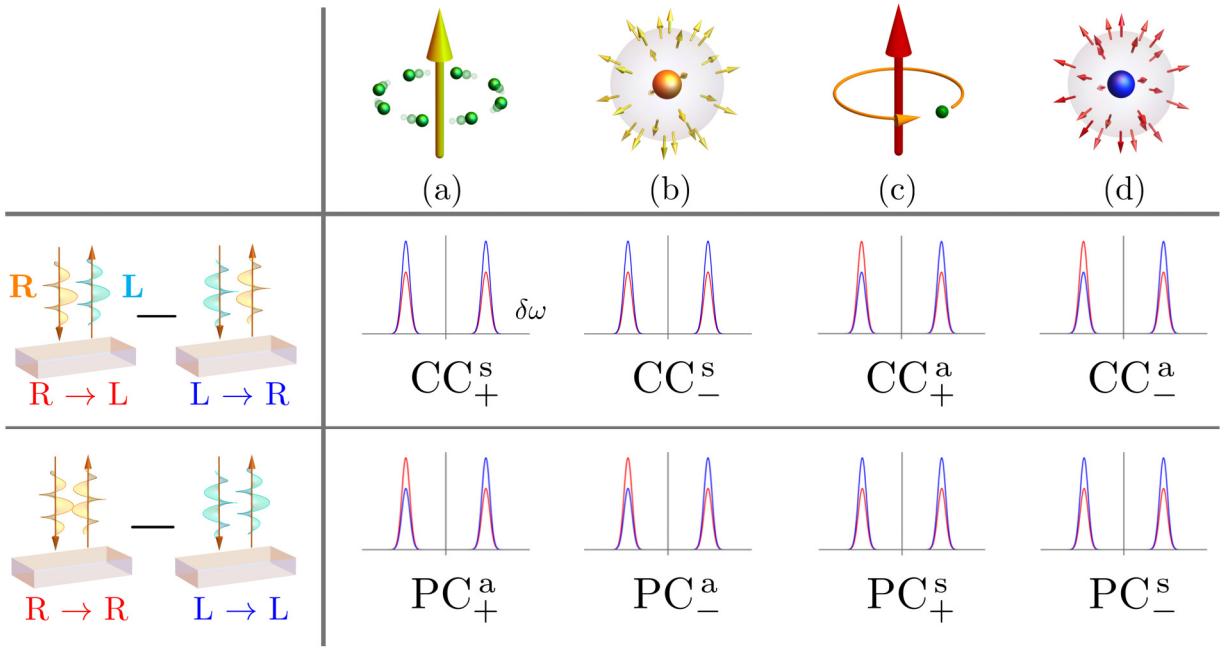

FIG. 2. Motifs of materials with the cross-circular Raman optical activity (CCROA) denoted by CC^{Y}_{X} and parallel-circular Raman optical activity (PCROA) denoted by PC^{Y}_{X} ($X = \pm, Y = \mathrm{s}, \mathrm{a}$). ROA is classified by the space-inversion (I) and time-reversal (θ) parities. For instance, the θ-even and θ-odd parts, respectively, point to the variations of the left-handed circularly polarized light response to the right-handed circularly polarized light (R→L, colored in red) and the right-handed one to the left-handed stimulus (L→R, colored in blue) in the identical and staggered manner between Stokes ($\delta\omega < 0$) and anti-Stokes ($\delta\omega > 0$) peaks. Note that we suppress the difference stemming from the Bose-Einstein distribution function [Eq. (20)]. (a) The even-parity and θ-even part ($\mathrm{CC}^{\mathrm{s}}_{+}$, $\mathrm{PC}^{\mathrm{a}}_{+}$) corresponds to the ferroaxial motif consisting of the circulating electric polarizations (green-colored spheres are displacing charges, yellow arrow denotes the ferroaxial vector $\boldsymbol{A}$). (b) The odd-parity and θ-even part ($\mathrm{CC}^{\mathrm{s}}_{-}$, $\mathrm{PC}^{\mathrm{a}}_{-}$) for the chiral motif formed by source or sink of ferroaxial vectors as $\nabla \cdot \boldsymbol{A}$ [67,68]. (c) The even-parity and θ-odd part ($\mathrm{CC}^{\mathrm{a}}_{+}$, $\mathrm{PC}^{\mathrm{s}}_{+}$) for the magnetoaxial motif such as magnetization $\boldsymbol{M}$ (red-colored arrow) associated with the circulating electric current colored in orange. (d) The odd-parity and θ-odd part ($\mathrm{CC}^{\mathrm{a}}_{-}$, $\mathrm{PC}^{\mathrm{s}}_{-}$) for the magnetic chiral motif represented by source or sink of magnetization, $\nabla \cdot \boldsymbol{M}$.

that all the classes in Eq. (38) do not allow for the even-parity CCROA.

The odd-parity CCROA for $\boldsymbol{q}_{\mathrm{i}} = [001]$ is classified by the class enhanced by the twofold rotation perpendicular to [001] or by n-fold rotation parallel to [001]. The obtained classes are

$$m\bar{3}m, 432, m\bar{3}m1', 4321', m'\bar{3}'m', \tag{39}$$

among which the composite-chiral (432), chiral ($4321'$), and magnetic chiral ($m'\bar{3}'m'$) cases imply CCROA.

Next, the incident direction is taken to be $\boldsymbol{q}_{\mathrm{i}} = [111]$. The odd-parity CCROA is similarly classified as that with $\boldsymbol{q}_{\mathrm{i}} = [001]$. After the enhancement of point groups with respect to the [111] direction, we obtain the same series of classes tabulated in Eq. (39). On the other hand, the even-parity CCROA for $\boldsymbol{q}_{\mathrm{i}} = [111]$ differs from that for $\boldsymbol{q}_{\mathrm{i}} = [001]$ where any magnetic Laue class of Eq. (38) does not possess the even-parity CCROA. The $m_{\perp}$ symmetry for the [111] incidence is not present in the colorless ($m\bar{3}$), gray ($m\bar{3}1'$), and black-white ($m\bar{3}m'$) classes, and thereby CCROA is allowed in spite of neither ferroaxial nor magnetoaxial anisotropy.

The obtained classification is summarized in Table III for the even-parity case and Table IV for the odd-parity case. Although we presented the symmetry analysis of CCROA, the classification for PCROA is the same as that for CCROA. The detailed analysis with the microscopic calculations is presented elsewhere [69].

VI. DISCUSSION

In this work, we investigated the symmetry of cross- and parallel-circular Raman optical activities and presented the systematic classification. The classification is obtained by the magnetic Laue class for the even-parity case and the (magneto)achiral/chiral crystal class for the odd-parity case. The result not only covers the cases identified in prior works on the ferroaxial, magnetoaxial, and chiral materials, but it also points out more diverse ROA, such as that from the magnetic chiral anisotropy. Moreover, the formulation is based on the phenomenological arguments applicable to various kinds of Raman-scattering processes, such as spontaneous and coherent stimulated Raman scatterings.

It is noteworthy that the antiunitary symmetry of solids is closely tied to the relation between the Stokes and anti-Stokes signals. Thus, the circular dichroism in the Raman scattering provides us with a powerful diagnosis of the symmetry of the target materials [70,71]. For example, it may be feasible to identify the antiunitary symmetry of the exotic quantum phase implied by the measurement of bulk properties [72,73]. The useful property is in stark contrast to that of nonlinear optical responses such as photocurrent generation, in which the

TABLE II. Classification of odd-parity CCROA (CC_-) by achiral (aC), chiral (C), magneto-achiral (m-aC), magnetic chiral (m-C), and composite-chiral (c-C) classes. Each class is labeled by the θ-even and θ-odd odd-parity CCROA; e.g., $(\times, \checkmark)$ denotes no θ-even CCROA, but θ-odd CCROA allowed. The notations for M, G, g are the same as those in Table I.

Class	Type	CCROA	M	G	g
$\bar{1}$	m-aC	$(\times, \times)$	$\bar{1}$	$\bar{1}$	
1	c-C	$(\checkmark, \checkmark)^*$	1	1	
$2/m$	m-aC	$(\times, \times)$	m	m	
			$2/m$	$2/m$	
2	c-C	$(\checkmark, \checkmark)^*$	2	2	
mmm	m-aC	$(\times, \times)$	mmm	mmm	
			$2mm$	$2mm$	
222	c-C	$(\checkmark, \checkmark)^*$	222	222	
$\bar{3}m$	m-aC	$(\times, \times)$	$\bar{3}$	$\bar{3}$	
			$3m$	$3m$	
			$\bar{3}m$	$\bar{3}m$	
32	c-C	$(\checkmark, \checkmark)$	3	3	
			32	32	
$4/mmm$	m-aC	$(\times, \times)$	$\bar{4}$	$\bar{4}$	
			$4/m$	$4/m$	
			$4mm$	$4mm$	
			$\bar{4}2m$	$\bar{4}2m$	
			$4/mmm$	$4/mmm$	
422	c-C	$(\checkmark, \checkmark)$	4	4	
			422	422	
$6/mmm$	m-aC	$(\times, \times)$	$\bar{6}$	$\bar{6}$	
			$6/m$	$6/m$	
			$6mm$	$6mm$	
			$\bar{6}2m$	$\bar{6}2m$	
			$6/mmm$	$6/mmm$	
622	c-C	$(\checkmark, \checkmark)$	6	6	
			622	622	
$1'$	C	$(\checkmark, \times)$	$1'$	1	1
$\bar{1}1'$	aC	$(\times, \times)$	$\bar{1}1'$	$\bar{1}$	1
$\bar{1}'$	m-C	$(\times, \checkmark)$	$\bar{1}'$	1	$\bar{1}$
$2/m1'$	aC	$(\times, \times)$	$2/m1'$	$2/m$	1
			$m1'$	m	1
			$2/m'$	$\bar{1}$	2
$21'$	C	$(\checkmark, \times)$	$21'$	2	1
			$2'$	1	2
$2/m'$	m-C	$(\times, \checkmark)$	$2/m'$	2	$\bar{1}$
			m'	1	m
$mmm1'$	aC	$(\times, \times)$	$mmm1'$	mmm	1
			$2mm1'$	$2mm$	1
			$m'm2'$	m	2
			$m'mm$	$2mm$	$\bar{1}$
			$m'm'm$	$2/m$	2
$2221'$	C	$(\checkmark, \times)$	$2221'$	222	1
			$2'2'2$	2	2
$m'm'm'$	m-C	$(\times, \checkmark)$	$m'm'm'$	222	$\bar{1}$
			$m'm'2$	2	m
$\bar{3}m1'$	aC	$(\times, \times)$	$\bar{3}m1'$	$\bar{3}m$	1
			$\bar{3}1'$	$\bar{3}$	1
			$3m1'$	$3m$	1
			$\bar{3}'m$	$3m$	$\bar{1}$
			$\bar{3}m'$	$\bar{3}$	m
$321'$	C	$(\checkmark, \times)$	$321'$	32	1
			$31'$	3	1
			$32'$	3	2
$\bar{3}'m'$	m-C	$(\times, \checkmark)$	$\bar{3}'m''$	32	$\bar{1}$
			$\bar{3}'$	3	$\bar{1}$
			$3m'$	3	m
$4/mmm1'$	aC	$(\times, \times)$	$4'/m$	$2/m$	$\bar{4}$
			$4'/m'$	$\bar{4}$	$\bar{1}$
			$4/m1'$	$4/m$	1
			$\bar{4}1'$	$\bar{4}$	1
			$\bar{4}2'm'$	$\bar{4}$	$m_\perp$
			$4/mm'm'$	$4/m$	$2_\perp$
			$4'/mmm'$	mmm	4
			$\bar{4}'2'm$	$2mm$	$\bar{4}$
			$4'mm'$	$2mm$	4
			$\bar{4}2m1'$	$\bar{4}2m$	1
			$4mm1'$	$4mm$	1
			$4/mmm1'$	$4/mmm$	1
			$4/m'mm$	$4mm$	$\bar{1}$
			$4'/m'm'm$	$\bar{4}2m$	$\bar{1}$
$4221'$	C	$(\checkmark, \times)$	$4'$	2	4
			$41'$	4	1
			$4'22'$	222	4
			$42'2'$	4	$2_\perp$
			$4221'$	422	1
$4/m'm'm'$	m-C	$(\times, \checkmark)$	$\bar{4}'$	2	$\bar{4}$
			$4/m'$	4	$\bar{1}$
			$4m'm'$	4	$m_\perp$
			$\bar{4}'2m'$	222	$\bar{4}$
			$4/m'm'm'$	422	$\bar{1}$
$6/mmm1'$	aC	$(\times, \times)$	$\bar{6}1'$	$\bar{6}$	1
			$6/m1'$	$6/m$	1
			$6'/m$	$\bar{6}$	$\bar{1}$
			$6'/m'$	$\bar{3}$	6
			$6mm1'$	$6mm$	1
			$\bar{6}2m1'$	$\bar{6}2m$	1
			$6/mmm1'$	$6/mmm$	1
			$6'/mmm'$	$\bar{6}m2$	$\bar{1}$
			$6/m'mm$	$6mm$	$\bar{1}$
			$\bar{6}m'2'$	$\bar{6}$	$2_\perp$
			$6/mm'm'$	$6/m$	$m_\perp$
			$\bar{6}'m2'$	$3m$	$2_\perp$
			$6'/m'm'm$	$\bar{3}m$	2
$6221'$	C	$(\checkmark, \times)$	$61'$	6	1
			$6'$	3	2
			$6221'$	622	1
			$62'2'$	6	$2_\perp$
			$6'2'2$	32	$2_\perp$
$6/m'm'm'$	m-C	$(\times, \checkmark)$	$6/m'$	6	$\bar{1}$
			$\bar{6}'$	3	$\bar{6}$
			$6/m'm'm'$	622	$\bar{1}$
			$\bar{6}'m'2$	32	$m_\perp$
			$6m'm'$	6	$m_\perp$
			$6'm'm$	32	$m_\perp$

different antiunitary symmetry (e.g., θ or θI symmetry) does not give qualitative differences while it implies the distinct mechanism for the response.

Tables I and II also show that both the θ-even and θ-odd ROA can occur in a certain case, such as that belonging to the colorless and axial Laue class (e.g., $M = \bar{6}$). It implies an

TABLE III. Classification of even-parity cross- and parallel-circular Raman optical activities (CC_+, PC_+) for the cubic systems. Each class is labeled by the θ-even and θ-odd ROA regarding the [001] and [111] incidence; e.g., $ROA_{[001]} = (\times, \checkmark)$ denotes no θ-even ROA but allowed θ-odd ROA for the incident light with $\boldsymbol{q}_i$ = [001]. Other notations are the same as those given in Table I.

Laue class	$ROA_{[001]}$	$ROA_{[111]}$	M	G	g
(colorless Laue class)					
$m\bar{3}m$	$(\times, \times)$	$(\times, \times)$	$\bar{4}3m$	$\bar{4}3m$	
			432	432	
			$m\bar{3}m$	$m\bar{3}m$	
$m\bar{3}$	$(\times, \times)$	$(\checkmark, \checkmark)$	23	23	
			$m\bar{3}$	$m\bar{3}$	
(gray and black-white Laue classes)					
$m\bar{3}m1'$	$(\times, \times)$	$(\times, \times)$	$\bar{4}3m1'$	$\bar{4}3m$	1
			$4321'$	432	1
			$m\bar{3}m1'$	$m\bar{3}m$	1
			$m'\bar{3}m'$	432	$\bar{1}$
			$m'\bar{3}m$	$\bar{4}3m$	$\bar{1}$
$m\bar{3}1'$	$(\times, \times)$	$(\checkmark, \times)$	$231'$	23	1
			$m\bar{3}1'$	$m\bar{3}$	1
			$m'\bar{3}'$	23	$\bar{1}$
$m\bar{3}m'$	$(\times, \times)$	$(\times, \checkmark)$	$\bar{4}'3m'$	23	m
			$4'32'$	23	4
			$m\bar{3}m'$	$m\bar{3}$	4

TABLE IV. Classification of odd-parity cross- and parallel-circular Raman optical activities (CC_-, PC_-) for the cubic systems. Each class is labeled by the θ-even and θ-odd ROA regarding the [001] and [111] incidence; e.g., ROA= $(\times, \checkmark)$ denotes no θ-even CCROA but allowed θ-odd ROA. Other notations are the same as those in Table II.

Laue class	Type	ROA	M	G	g
$m\bar{3}m$	m-aC	$(\times, \times)$	$m\bar{3}$	$m\bar{3}$	
			$\bar{4}3m$	$\bar{4}3m$	
			$m\bar{3}m$	$m\bar{3}m$	
432	c-C	$(\checkmark, \times)$	23	23	
			432	432	
$m\bar{3}m1'$	aC	$(\times, \times)$	$m\bar{3}1'$	$m\bar{3}$	1
			$\bar{4}3m1'$	$\bar{4}3m$	1
			$m\bar{3}m1'$	$m\bar{3}m$	1
			$m'\bar{3}m$	$\bar{4}3m$	$\bar{1}$
			$m\bar{3}m'$	$m\bar{3}$	4
$4321'$	C	$(\checkmark, \times)$	$231'$	23	1
			$4321'$	432	1
			$4'32'$	23	4
$m'\bar{3}'m'$	mC	$(\times, \checkmark)$	$m'\bar{3}'$	23	$\bar{1}$
			$m'\bar{3}m'$	432	$\bar{1}$
			$\bar{4}'3m'$	23	m

intriguing situation that ROA is found in only the Stokes or anti-Stokes peak since the θ-even and θ-odd parts contribute to those peaks in a constructive or destructive manner. Such "perfect" CCROA and PCROA may be realized in ferroaxial materials under large magnetic fields or by combining with the magnetoaxial order (e.g., ferromagnetic order). The phenomenon may be feasible for the odd-parity case (see the composite-chiral class in Table II).

The quantitative aspects of responses are an important issue to be addressed. We expect that our symmetry analysis will be useful for exploring significant CCROA and PCROA with those microscopic calculations.

ACKNOWLEDGMENTS

H.W. is grateful to Eiichi Oishi for helpful discussions. R.O. was supported by Special Postdoctoral Researcher Program at RIKEN. This work is supported by Grant-in-Aid for Scientific Research from JSPS KAKENHI, Grant No. JP23K13058 (H.W.), No. JP24K00581 (H.W.), No. JP25H02115 (H.W.), No. JP21H04990 (R.A.), No. JP25H01246 (R.A.), No. JP25H01252 (R.A.), JST-CREST No. JPMJCR23O4(R.A.), JST-ASPIRE No. JPMJAP2317 (R.A.), JST-Mirai No. JPMJMI20A1 (R.A.), MEXT X-NICS No. JPJ011438 (T.S.), NINS OML Project No. OML012301 (T.S.), JST CREST No. JPMJCR24R5 (T.S.), and RIKEN TRIP initiative (RIKEN Quantum, Advanced General Intelligence for Science Program, Many-body Electron Systems). H.W. was also supported by JSR Corporation via JSR-UTokyo Collaboration Hub, CURIE.

DATA AVAILABILITY

The data that support the findings of this article are not publicly available upon publication because it is not technically feasible and/or the cost of preparing, depositing, and hosting the data would be prohibitive within the terms of this research project. The data are available from the authors upon reasonable request.

[1] R. Loudon, The Raman effect in crystals, Adv. Phys. **50**, 813 (2001).

[2] P. Y. Yu and M. Cardona, *Fundamentals of Semiconductors: Physics and Materials Properties*, 4th ed., Graduate Texts in Physics (Springer, Berlin, 2010).

[3] R. L. Greene, D. D. Sell, W. M. Yen, A. L. Schawlow, and R. M. White, Observation of a spin-wave sideband in the optical spectrum of MnF_2, Phys. Rev. Lett. **15**, 656 (1965).

[4] Y. Tanabe, T. Moriya, and S. Sugano, Magnon-induced electric dipole transition moment, Phys. Rev. Lett. **15**, 1023 (1965).

[5] P. A. Fleury and R. Loudon, Scattering of light by one- and two-magnon excitations, Phys. Rev. **166**, 514 (1968).

[6] W. Jin, H. H. Kim, Z. Ye, S. Li, P. Rezaie, F. Diaz, S. Siddiq, E. Wauer, B. Yang, C. Li, S. Tian, K. Sun, H. Lei, A. W. Tsen, L. Zhao, and R. He, Raman fingerprint of two terahertz spin wave branches in a two-dimensional honeycomb Ising ferromagnet, Nat. Commun. **9**, 5122 (2018).

[7] W. Jin, Z. Ye, X. Luo, B. Yang, G. Ye, F. Yin, H. H. Kim, L. Rojas, S. Tian, Y. Fu, S. Yan, H. Lei, K. Sun, A. W. Tsen, R. He, and L. Zhao, Tunable layered-magnetism-assisted

magneto-Raman effect in a two-dimensional magnet CrI_3, Proc. Natl. Acad. Sci. USA **117**, 24664 (2020).

[8] A. McCreary, T. T. Mai, F. G. Utermohlen, J. R. Simpson, K. F. Garrity, X. Feng, D. Shcherbakov, Y. Zhu, J. Hu, D. Weber, K. Watanabe, T. Taniguchi, J. E. Goldberger, Z. Mao, C. N. Lau, Y. Lu, N. Trivedi, R. Valdés Aguilar, and A. R. Hight Walker, Distinct magneto-Raman signatures of spin-flip phase transitions in CrI_3, Nat. Commun. **11**, 3879 (2020).

[9] Y. Zhang, X. Wu, B. Lyu, M. Wu, S. Zhao, J. Chen, M. Jia, C. Zhang, L. Wang, X. Wang, Y. Chen, J. Mei, T. Taniguchi, K. Watanabe, H. Yan, Q. Liu, L. Huang, Y. Zhao, and M. Huang, Magnetic order-induced polarization anomaly of Raman scattering in 2D magnet CrI_3, Nano Lett. **20**, 729 (2020).

[10] B. Huang, J. Cenker, X. Zhang, E. L. Ray, T. Song, T. Taniguchi, K. Watanabe, M. A. McGuire, D. Xiao, and X. Xu, Tuning inelastic light scattering via symmetry control in the two-dimensional magnet CrI_3, Nat. Nanotechnol. **15**, 212 (2020).

[11] D. Lujan, J. Choe, M. Rodriguez-Vega, Z. Ye, A. Leonardo, T. N. Nunley, L.-J. Chang, S.-F. Lee, J. Yan, G. A. Fiete, R. He, and X. Li, Magnons and magnetic fluctuations in atomically thin $MnBi_2Te_4$, Nat. Commun. **13**, 2527 (2022).

[12] N. Koshizuka, S. Ushioda, and T. Tsushima, Resonance Raman scattering in $CdCr_2S_4$: Magnetic-circular-polarization properties, Phys. Rev. B **21**, 1316 (1980).

[13] J. Cenker, B. Huang, N. Suri, P. Thijssen, A. Miller, T. Song, T. Taniguchi, K. Watanabe, M. A. McGuire, D. Xiao, and X. Xu, Direct observation of two-dimensional magnons in atomically thin CrI_3, Nat. Phys. **17**, 20 (2021).

[14] E. M. Lacinska, M. Furman, J. Binder, I. Lutsyk, P. J. Kowalczyk, R. Stepniewski, and A. Wysmolek, Raman optical activity of 1T-TaS_2, Nano Lett. **22**, 2835 (2022).

[15] H. F. Yang, K. Y. He, J. Koo, S. W. Shen, S. H. Zhang, G. Liu, Y. Z. Liu, C. Chen, A. J. Liang, K. Huang, M. X. Wang, J. J. Gao, X. Luo, L. X. Yang, J. P. Liu, Y. P. Sun, S. C. Yan, B. H. Yan, Y. L. Chen, X. Xi *et al.*, Visualization of chiral electronic structure and anomalous optical response in a material with chiral charge density waves, Phys. Rev. Lett. **129**, 156401 (2022).

[16] G. Liu, T. Qiu, K. He, Y. Liu, D. Lin, Z. Ma, Z. Huang, W. Tang, J. Xu, K. Watanabe, T. Taniguchi, L. Gao, J. Wen, J.-M. Liu, B. Yan, and X. Xi, Electrical switching of ferro-rotational order in nanometre-thick 1T-TaS_2 crystals, Nat. Nanotechnol. **18**, 854 (2023).

[17] Y. Zhao, Z. Nie, H. Hong, X. Qiu, S. Han, Y. Yu, M. Liu, X. Qiu, K. Liu, S. Meng, L. Tong, and J. Zhang, Spectroscopic visualization and phase manipulation of chiral charge density waves in 1T-TaS_2, Nat. Commun. **14**, 2223 (2023).

[18] V. A. Martinez, Y. Gao, J. Yang, F. Lyzwa, Z. Liu, C. J. Won, K. Du, V. Kiryukhin, S. W. Cheong, and A. A. Sirenko, Ferroaxial phonons in chiral and polar $NiCo_2TeO_6$, Phys. Rev. B **112**, 064411 (2025).

[19] K. Ishito, H. Mao, Y. Kousaka, Y. Togawa, S. Iwasaki, T. Zhang, S. Murakami, J. Kishine, and T. Satoh, Truly chiral phonons in α-HgS, Nat. Phys. **19**, 35 (2023).

[20] K. Ishito, H. Mao, K. Kobayashi, Y. Kousaka, Y. Togawa, H. Kusunose, J. Kishine, and T. Satoh, Chiral phonons: Circularly polarized Raman spectroscopy and *ab initio* calculations in a chiral crystal tellurium, Chirality **35**, 338 (2023).

[21] E. Oishi, Y. Fujii, and A. Koreeda, Selective observation of enantiomeric chiral phonons in α-quartz, Phys. Rev. B **109**, 104306 (2024).

[22] M. Vargek, T. B. Freedman, and L. A. Nafie, Improved backscattering dual circular polarization raman optical activity spectrometer with enhanced performance for biomolecular applications, J. Raman Spectrosc. **28**, 627 (1997).

[23] L. A. Nafie and T. B. Freedman, Dual circular polarization Raman optical activity, Chem. Phys. Lett. **154**, 260 (1989).

[24] J. A. Koningstein and O. S. Mortensen, Experimental observation of an antisymmetric Raman scattering tensor, Nature (London) **217**, 445 (1968).

[25] O. S. Mortensen and J. A. Koningstein, Electronic Raman effect. II. Asymmetry of the scattering tensor for electronic Raman transitions, J. Chem. Phys. **48**, 3971 (1968).

[26] L. D. Barron and A. D. Buckingham, Rayleigh and Raman scattering from optically active molecules, Mol. Phys. **20**, 1111 (1971).

[27] Y.-N. Chiu, Theory of a novel odd-parity Raman scattering mechanism: Depolarization ratios and reversal coefficients for random molecular systems, J. Chem. Phys. **52**, 3641 (1970).

[28] L. D. Barron and A. D. Buckingham, Rayleigh and Raman optical activity, Annu. Rev. Phys. Chem. **26**, 381 (1975).

[29] G. Kusuno, T. Hayashida, T. Nagai, H. Watanabe, R. Oiwa, T. Kimura, and T. Satoh, Raman optical activity induced by ferroaxial order in $NiTiO_3$, arXiv:2505.22488.

[30] L. N. Ovander, The form of the Raman tensor, Opt. Spectrosc. **9**, 302 (1960).

[31] A. P. Cracknell, Scattering matrices for the Raman effect in magnetic crystals, J. Phys. **2**, 500 (1969).

[32] S. P. S. Porto, J. A. Giordmaine, and T. C. Damen, Depolarization of Raman scattering in calcite, Phys. Rev. **147**, 608 (1966).

[33] K. R. Hoffman, W. M. Yen, D. J. Lockwood, and P. E. Sulewski, Birefringence-induced vibrational Raman and Rayleigh optical activity in uniaxial crystals, Phys. Rev. B **49**, 182 (1994).

[34] S. Zhang, N. Mao, N. Zhang, J. Wu, L. Tong, and J. Zhang, Anomalous polarized Raman scattering and large circular intensity differential in layered triclinic ReS_2, ACS Nano **11**, 10366 (2017).

[35] S. Naguleswaran and G. E. Stedman, Onsager relations and time-reversal symmetry in nonlinear optics, J. Phys. B **31**, 935 (1998).

[36] R. Loudon, Time-reversal symmetry in light-scattering theory, J. Raman Spectrosc. **7**, 10 (1978).

[37] L. Hecht and L. D. Barron, Time reversal and hermiticity characteristics of polarizability and optical activity operators, Mol. Phys. **79**, 887 (1993).

[38] L. D. Barron, Anti-stokes Raman optical activity, Mol. Phys. **31**, 1929 (1976).

[39] L. D. Barron and J. R. Escribano, Stokes–antiStokes asymmetry in natural Raman optical activity, Chem. Phys. **98**, 437 (1985).

[40] L. D. Barron and J. Vrbancich, Anti-stokes magnetic Raman optical activity and time reversal, Chem. Phys. Lett. **92**, 466 (1982).

[41] R. D. Johnson, S. Nair, L. C. Chapon, A. Bombardi, C. Vecchini, D. Prabhakaran, A. T. Boothroyd, and P. G. Radaelli, $Cu_3Nb_2O_8$: A multiferroic with chiral coupling to the crystal structure, Phys. Rev. Lett. **107**, 137205 (2011).

[42] J. Hlinka, J. Privratska, P. Ondrejkovic, and V. Janovec, Symmetry guide to ferroaxial transitions, Phys. Rev. Lett. **116**, 177602 (2016).

[43] S. Hayami, R. Oiwa, and H. Kusunose, Electric ferro-axial moment as nanometric rotator and source of longitudinal spin current, J. Phys. Soc. Jpn. **91**, 113702 (2022).

[44] S. Yamagishi, T. Hayashida, R. Misawa, K. Kimura, M. Hagihala, T. Murata, S. Hirose, and T. Kimura, Ferroaxial transitions in glaserite-type compounds: Database screening, phonon calculations, and experimental verification, Chem. Mater. **35**, 747 (2023).

[45] S. Bhowal and N. A. Spaldin, Electric toroidal dipole order and hidden spin polarization in ferroaxial materials, Phys. Rev. Res. **6**, 043141 (2024).

[46] Z. He and G. Khalsa, Optical control of ferroaxial order, Phys. Rev. Res. **6**, 043220 (2024).

[47] E. Day-Roberts, R. M. Fernandes, and T. Birol, Piezoresistivity as a fingerprint of ferroaxial transitions, Phys. Rev. Lett. **134**, 016401 (2025).

[48] M. Kenzelmann, G. Lawes, A. B. Harris, G. Gasparovic, C. Broholm, A. P. Ramirez, G. A. Jorge, M. Jaime, S. Park, Q. Huang, A. Y. Shapiro, and L. A. Demianets, Direct transition from a disordered to a multiferroic phase on a triangular lattice, Phys. Rev. Lett. **98**, 267205 (2007).

[49] W. Jin, E. Drueke, S. Li, A. Admasu, R. Owen, M. Day, K. Sun, S.-W. Cheong, and L. Zhao, Observation of a ferro-rotational order coupled with second-order nonlinear optical fields, Nat. Phys. **16**, 42 (2020).

[50] T. Hayashida, Y. Uemura, K. Kimura, S. Matsuoka, D. Morikawa, S. Hirose, K. Tsuda, T. Hasegawa, and T. Kimura, Visualization of ferroaxial domains in an order-disorder type ferroaxial crystal, Nat. Commun. **11**, 4582 (2020).

[51] D. Sekine, T. Sato, Y. Tokunaga, T.-h. Arima, and M. Matsubara, Second harmonic imaging of antiferromagnetic domains and confirmation of absence of ferroaxial twins in $MnTiO_3$, Phys. Rev. Mater. **8**, 064406 (2024).

[52] X. Zhang, T. Carbin, K. Du, B. Li, K. Wang, C. Li, T. Qian, N. Ni, S.-W. Cheong, and A. Kogar, Directionally asymmetric nonlinear optics in planar chiral $MnTiO_3$, arXiv:2410.18086.

[53] H. Hanate, T. Hasegawa, S. Hayami, S. Tsutsui, S. Kawano, and K. Matsuhira, First observation of superlattice reflections in the hidden order at 105 K of spin–orbit coupled iridium oxide $Ca_5Ir_3O_{12}$, J. Phys. Soc. Jpn. **90**, 063702 (2021).

[54] H. Hanate, S. Tsutsui, T. Yajima, H. Nakao, H. Sagayama, T. Hasegawa, and K. Matsuhira, Space-group determination of superlattice structure due to electric toroidal ordering in $Ca_5Ir_3\ O_{12}$, J. Phys. Soc. Jpn. **92**, 063601 (2023).

[55] S. Hayami, S. Tsutsui, H. Hanate, N. Nagasawa, Y. Yoda, and K. Matsuhira, Cluster toroidal multipoles formed by electric-quadrupole and magnetic-octupole trimers: A possible scenario for hidden orders in $Ca_5Ir_3O_{12}$, J. Phys. Soc. Jpn. **92**, 033702 (2023).

[56] Y. Kajita, T. Nagai, S. Yamagishi, K. Kimura, M. Hagihala, and T. Kimura, Ferroaxial transitions in glaserite-type $Na_2\ BaM(PO_4)_2$ (M = Mg, Mn, Co, and Ni), Chem. Mater. **36**, 7451 (2024).

[57] Y. Kajita, T. Hayashida, S. Yamagishi, K. Kimura, and T. Kimura, Ferroaxial domain imaging in glaserite-type $Na_2\ BaM(PO_4)_2$ (M = Mg, Mn, Co, and Ni), J. Phys. Soc. Jpn. **94**, 063702 (2025).

[58] X. Song, L. Liu, Y. Chen, H. Yang, Z. Huang, B. Hou, Y. Hou, X. Han, H. Yang, Q. Zhang, T. Zhang, J. Zhou, Y. Huang, Y. Zhang, H.-J. Gao, and Y. Wang, Atomic-scale visualization of chiral charge density wave superlattices and their reversible switching, Nat. Commun. **13**, 1843 (2022).

[59] A. A. Sirenko, T. Ruf, M. Cardona, D. R. Yakovlev, W. Ossau, A. Waag, and G. Landwehr, Electron and holegfactors measured by spin-flip Raman scattering in $CdTe/Cd_{1-x}Mg_xTe$ single quantum wells, Phys. Rev. B **56**, 2114 (1997).

[60] P. Kossacki, C. Faugeras, M. Kühne, M. Orlita, A. Mahmood, E. Dujardin, R. R. Nair, A. K. Geim, and M. Potemski, Circular dichroism of magnetophonon resonance in doped graphene, Phys. Rev. B **86**, 205431 (2012).

[61] S. Nakatsuji and R. Arita, Topological magnets: Functions based on berry phase and multipoles, Annu. Rev. Condens. Matter Phys. **13**, 119 (2022).

[62] L. Šmejkal, A. H. MacDonald, J. Sinova, S. Nakatsuji, and T. Jungwirth, Anomalous Hall antiferromagnets, Nat. Rev. Mater. **7**, 482 (2022).

[63] L. D. Barron, True and false chirality and absolute asymmetric synthesis, J. Am. Chem. Soc. **108**, 5539 (1986).

[64] D. Che, L. Hecht, and L. A. Nafie, Dual and incident circular polarization Raman optical activity backscattering of (–)-trans-pinane, Chem. Phys. Lett. **180**, 182 (1991).

[65] H. Watanabe and Y. Yanase, Magnetic parity violation and parity-time-reversal-symmetric magnets, J. Phys.: Condens. Matter **36**, 373001 (2024).

[66] M. I. Aroyo, *International Tables for Crystallography*, Space-Group Symmetry, Vol. A (Springer, 2016).

[67] R. Oiwa and H. Kusunose, Rotation, electric-field responses, and absolute enantioselection in chiral crystals, Phys. Rev. Lett. **129**, 116401 (2022).

[68] R. Oiwa and H. Kusunose, Predominant electronic order parameter for structural chirality – role of spinless electronic toroidal multipoles, arXiv:2504.11682.

[69] H. Watanabe, R. Oiwa, and R. Arita, Dual-circular Raman optical activity of axial multipolar order, arXiv:2507.09237.

[70] H.-H. Kung, R. E. Baumbach, E. D. Bauer, V. K. Thorsmølle, W.-L. Zhang, K. Haule, J. A. Mydosh, and G. Blumberg, Heavy fermions. Chirality density wave of the "hidden order" phase in URu_2Si_2, Science **347**, 1339 (2015).

[71] H.-H. Kung, S. Ran, N. Kanchanavatee, V. Krapivin, A. Lee, J. A. Mydosh, K. Haule, M. B. Maple, and G. Blumberg, Analogy between the "hidden order" and the orbital antiferromagnetism in $URu_{2-x}Fe_xSi_2$, Phys. Rev. Lett. **117**, 227601 (2016).

[72] L. Zhao, C. A. Belvin, R. Liang, D. A. Bonn, W. N. Hardy, N. P. Armitage, and D. Hsieh, A global inversion-symmetry-broken phase inside the pseudogap region of $YBa_2Cu_3O_y$, Nat. Phys. **13**, 250 (2017).

[73] H. Murayama, K. Ishida, R. Kurihara, T. Ono, Y. Sato, Y. Kasahara, H. Watanabe, Y. Yanase, G. Cao, Y. Mizukami, T. Shibauchi, Y. Matsuda, and S. Kasahara, Bond directional anapole order in a spin-orbit coupled Mott insulator $Sr_2(Ir_{1-x}Rh_x)O_4$, Phys. Rev. X **11**, 011021 (2021).